PAPER

Check for updates

Gas phase *vs.* liquid phase: monitoring H₂ and CO adsorption phenomena on Pt/Al₂O₃ by IR spectroscopy

Michele Carosso,[a] Thibault Fovanna,[b] Alberto Ricchebuono,[a] Eleonora Vottero, [iD][a] Maela Manzoli, [iD][c] Sara Morandi, [iD][a] Riccardo Pellegrini,[d] Andrea Piovano, [iD][e] Davide Ferri [iD]*[b] and Elena Groppo [iD]*[a]

The adsorption phenomena occurring at the surface of a highly-dispersed Pt/Al₂O₃ catalyst for hydrogenation reactions were thoroughly investigated in the gas-phase by transmission IR spectroscopy and in the liquid-phase by ATR-IR spectroscopy. The reduction of Pt/Al₂O₃ in H₂ with the formation of Pt–hydrides and adsorption of CO were used as case studies for the comparison of the two different environments under otherwise similar experimental conditions. We found that compared to gas-phase, the selected solvent (cyclohexane) greatly affects the reducibility of Pt. Incomplete reduction under the adopted liquid-phase conditions was demonstrated by the formation of carbonate species at very low CO coverage. Moreover, cyclohexane competes with the adsorbates (H₂ as well as CO) for the occupancy of the available surface sites, thus affecting the shape, position and relative intensity of the infrared signals corresponding to the surface Pt–H and Pt–CO species and leading to an overall lower H and/or CO coverage. Our spectroscopic data show also that the presence of the solvent is crucial in maintaining the Pt nanoparticles in partially H-solvated state even in a H₂-free environment. This evidence might have important implications with respect to the catalyst reactivity and stability.

1. Introduction

Platinum based catalysts are massively employed in industrial processes involving hydrogenation reactions, such as in the synthesis of specialty chemicals and drugs.[1–4] This is largely due to the superior ability of platinum in splitting molecular hydrogen into its atomic form.[5,6] Understanding the nature and the behaviour of the platinum hydride (Pt–H) species under reaction conditions is crucial to design more efficient and profitable catalysts. However, characterizing the phenomena occurring at the surface of supported metal nanoparticles is one of the main challenges in surface science, due to the combination of many factors, among which are the intrinsic complexity of metal nanoparticles[7–13] and their dynamic behaviour in the presence of adsorbates.[14–24] In this context, the H₂@Pt system was extensively investigated both theoretically[15,16,21,24–28] and

experimentally, especially by means of X-ray absorption spectroscopy (XAS),[13,14,17,18,22,25,29–36] IR spectroscopy[37–43] and inelastic neutron scattering (INS) spectroscopy.[44–48] While XAS provides direct information on the structural and electronic changes experienced by nanometric Pt particles in the presence of hydrogen, vibrational spectroscopies have the capability to discern between different Pt–H surface species, since the Pt–H vibration is sensitive to even small changes in the coordination geometry.

In such a scenario, some of us were involved in a systematic investigation of the hydride species formed over an industrial Pt/Al₂O₃ catalyst as a function of the H-coverage in the gas-phase, exploiting a multi-technique approach comprising INS, FT-IR and synchronous DRIFT/XAS/MS.[49] INS, being extremely sensitive towards vibrational modes involving hydrogen motion and almost silent towards all other elements, allowed the detection of the vibrational fingerprints of multi-coordinated Pt–H species under high H-coverage conditions, which are not visible by FT-IR spectroscopy because they fall in the spectral region dominated by the vibrational modes of the alumina framework. By comparison, because the threshold of absorption of MgO is at lower energy, multi-folded hydrides were observed on Pt/MgO.[50] By *operando* DRIFT/XAS/MS we were able to distinguish with an unprecedented level of detail

[a] Department of Chemistry, INSTM and NIS Centre, University of Torino, via Quarello 15/A, I-10135 Torino, Italy. E-mail: elena.groppo@unito.it
[b] Paul Scherrer Institut, 5232 Villigen PSI, Switzerland. E-mail: davide.ferri@psi.ch
[c] Department of Drug Science and Technology, INSTM and NIS Centre, University of Torino, via Pietro Giuria 9, I-10125 Torino, Italy
[d] Chimet SpA – Catalyst Division, via di Pescaiola 74, I-52041, Viciomaggio Arezzo, Italy
[e] Institut Laue-Langevin (ILL), 71 avenue des Martyrs, 38000 Grenoble, France

This journal is © The Royal Society of Chemistry 2022

Catal. Sci. Technol., 2022, **12**, 1359–1367 | **1359**

at least four different species of linear Pt–hydrides characterized by different adsorption strengths and local environment, and to follow their interconversion into multi-coordinated Pt–H species upon changing the H-coverage.[49] This phenomenon was correlated with a structural and electronic reconstruction of the Pt nanoparticles, in good agreement with theoretical predictions.[15,16,21,24,25,27] It should be mentioned for the sake of clarity that the assignment of the IR signals in the 2100–1700 cm^{-1} to Pt–H species rather than to adsorbed CO is unambiguously confirmed by identical experiments with D_2, which shifts them to the 1600–1200 cm^{-1} region.[49]

Industrial reactions are often carried out in a liquid solvent and the transferability of the results obtained in the gas-phase to liquid-phase cannot be assumed *a priori*. In order to close the gap of knowledge between gas-phase and liquid-phase conditions, similar experiments should be performed in the presence of a solvent. Unfortunately, the reports dealing with the vibrational characterization of Pt–hydrides at a solid–liquid interface are rare,[43] likely because of technical limitations.[51] In the liquid phase, the absorption bands related to the solvent can be orders of magnitude more intense than those associated with the adsorbed species. In this context, attenuated total reflection IR (ATR-IR) spectroscopy offers interesting opportunities.[52] The catalyst can be deposited as a thin layer on the ATR crystal and contacted with the solvent. By exploiting this geometry, the amount of liquid sampled by the IR radiation is very small and most of the information is retrieved from the catalyst surface.[53–59] Nevertheless only very few studies dealing with a detailed characterization of Pt-based catalysts in organic solvents and/or water are available,[60] and they mainly focused on the use of CO as a molecular probe.[61–63] As a further consequence of the lack of studies in liquid-phase environment a systematic comparison between gas-phase and liquid-phase experiments performed on the same catalyst is rare.[94]

In this work, we bridged this gap of knowledge in the characterization of surface phenomena occurring at solid–gas and solid–liquid interfaces, by thoroughly investigating a highly-dispersed Pt/Al$_2$O$_3$ catalyst during H$_2$ and CO adsorption using transmission IR spectroscopy for the gas-phase and ATR-IR spectroscopy for the liquid-phase.

2. Experimental

2.1 Catalyst synthesis and preliminary characterization

The 5 wt% Pt/Al$_2$O$_3$ catalyst was prepared in the laboratories of the Catalyst Division of Chimet S.p.A., adopting a high-surface-area transitional alumina as a support (specific surface area = 116 m^2 g^{-1}; pore volume = 0.41 cm^3 g^{-1}) and following a proprietary deposition–precipitation method similar to the one reported by Kaprielova *et al.*[64] After preparation, the sample was carefully washed with water and dried at 120 °C overnight. The nominal Pt dispersion (D = 63%) was determined by a H$_2$/O$_2$ titration method.[65] As previously reported,[49] HR-TEM micrographs showed very

small and homogeneously distributed Pt nanoparticles, with an almost spherical shape and a regular size. A representative HR-TEM micrograph is reported in Fig. 1A, while Fig. 1B shows the particle size distribution obtained from the analysis of more than 700 particles. The average value (1.4 ± 0.4 nm) is in good agreement with the dispersion determined by H$_2$/O$_2$ titration, and was previously confirmed also by EXAFS data analysis.[49] Temperature programmed reduction (TPR) was performed to evaluate the reducibility of the Pt phase. The main reduction peak (Fig. 1C), which is due to the Pt^{2+} → Pt^0 reduction, starts at a temperature as low as −30 °C, reaches its maximum around 55 °C and ends around 130 °C. The integrated area below the peak delivers the overall hydrogen consumed in the process: it accounts for a Pt/H ratio of 3.6, indicating that the majority of the Pt phase was in the PtO$_2$ form in the pristine catalyst.

2.2 Methods

2.2.1 IR experiments in gas-phase.
For the H$_2$ adsorption experiment, about 10 mg of undiluted Pt/Al$_2$O$_3$ were pressed into a self-supported pellet and placed inside a commercial FT-IR reactor cell (AABSPEC, no. 2000-A multimode), which allows sample activation and collection of FT-IR spectra under controlled temperature and atmosphere. In our previous work[49] we demonstrated that the large dead volume of the cell allows exchanging the gas composition at a low rate, thus permitting to follow the intermediate steps in the dynamic behavior of the Pt nanoparticles as a function of the gas concentration. On the other hand, the large internal volume makes the gas flow dynamics poorly predictable. The catalyst was heated up to 70 °C (heating rate 5 °C min^{-1}) under an inert stream (N$_2$, 50 mL min^{-1}) and left at this temperature for *ca.* 30 min in order to desorb most of the physisorbed water before collecting a FT-IR spectrum. Then, the catalyst was contacted at the same temperature with a N$_2$/H$_2$ flow (50 mL min^{-1}, 10 vol% H$_2$) and FT-IR spectra were acquired every 10 s for about 10 min until saturation of the signals of surface hydride species. Finally, the gas flow composition was changed back to pure N$_2$ to monitor the H$_2$ desorption step: FT-IR spectra were collected continuously for approximately 70 min.

The CO adsorption experiment was performed in static conditions. The self-supported pellet was inserted into a gold envelope and successively placed inside a homemade quartz cell equipped with KBr windows, allowing for the sample activation in the 25–700 °C range and successive measurements at room temperature, in the 10^{-4}–10^3 mbar pressure range. The sample was heated up to 70 °C in dynamic vacuum and left at this temperature up to a final vacuum of 10^{-4} mbar. Successive reduction was performed by dosing an excess of H$_2$ (equilibrium pressure of p_{H_2} = 100 mbar, 2 times × 15 min) over the sample, followed by a final dynamic vacuum treatment down to 10^{-4} mbar. A FT-IR spectrum was collected at room temperature before contacting the sample at room temperature with pulses of a
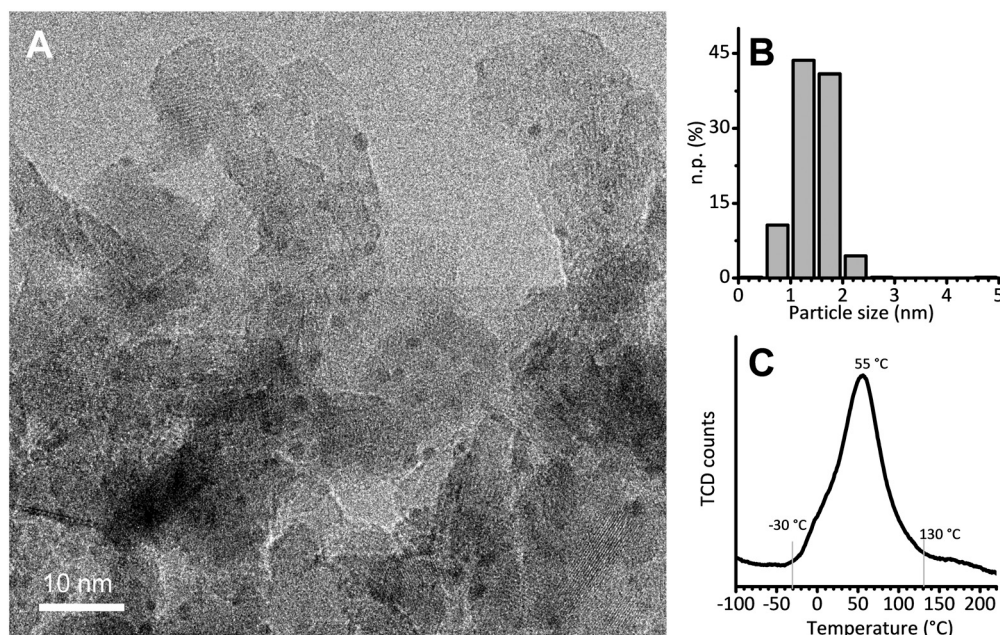
1360 | *Catal. Sci. Technol.*, 2022, **12**, 1359–1367

This journal is © The Royal Society of Chemistry 2022

Fig. 1 (A) Representative HR-TEM micrograph of Pt/Al$_2$O$_3$ (instrumental magnification 200 000X). (B) Corresponding particle size distribution determined by analysing more than 700 particles. (C) H$_2$-TPR.

10 vol% CO/He mixture up to an equilibrium pressure of $p_{He/CO}$ = 30 mbar. An IR spectrum was collected at each pulse.

For the experiments in gas-phase the FT-IR spectra were collected with a Bruker Invenio IR spectrometer equipped with a MCT detector by averaging 32 scans at 2 cm^{-1} resolution.

2.2.2 IR experiments in liquid-phase. For the *in situ* ATR-IR experiments, a slurry of the Pt/Al$_2$O$_3$ powder catalyst (*ca.* 10 mg) in Milli-Q water (*ca.* 1 mL) was dropped on the ZnSe internal reflection element (IRE; 90 × 10 × 10 mm) and dried overnight in a fume hood. The dried catalyst layer was then inserted into a horizontal ATR-IR cell working in continuous flow and whose temperature was regulated using a recirculating water bath. Cyclohexane was selected as the solvent, because it does not exhibit major absorptions in the spectral region of interest and it is considered relatively innocent, contrary to other solvents *e.g.* alcohols.[66,67] For the H$_2$ adsorption experiment, the catalyst was heated up to 70 °C under a continuous flow of Ar-saturated cyclohexane using a peristaltic pump (Ismatec) and left at 70 °C for 5 min. A first spectrum was collected and used as background. Then, the sample was contacted at the same temperature with H$_2$-saturated cyclohexane. ATR-IR spectra were recorded every minute for 60 min before switching the flow to Ar-saturated cyclohexane in order to investigate the stability of the adsorbates.

For the CO adsorption experiment, the catalyst layer was reduced in H$_2$ at 70 °C as described above, then cooled to room temperature in Ar-saturated cyclohexane and contacted with cyclohexane saturated with a 5 vol% CO/Ar mixture.

ATR-IR spectra were recorded continuously every minute for 60 min.

All the measurements were performed with a Bruker Vertex70 spectrometer equipped with a MCT detector and a commercial ATR mirror unit. The ATR-IR spectra were collected by accumulating 20 scans at 4 cm^{-1} resolution.

3. Results and discussion

3.1 Pt–Hydrides formation and dynamics upon reducing the H-coverage

Fig. 2A shows the sequence of IR spectra collected during gas-phase reduction of Pt/Al$_2$O$_3$ at 70 °C in the region characteristic for the ν(Pt–H) vibrational modes of linear Pt–H species. For the sake of clarity, this experiment is equivalent to the one reported in our previous work,[49] but performed at 70 °C instead of 120 °C in order to allow for a direct comparison with the experiments in the liquid phase. As soon as the catalyst was contacted by the N$_2$/H$_2$ flow, the growth of bands in the ν(OH) and δ(OH) region (not shown) testified the formation of H$_2$O that was accompanied by the simultaneous appearance of a few weak bands in the ν(Pt–H) region. According to the literature[37–43] and following our previous work,[49] band I at 2115 cm^{-1} (which is detectable only in the presence of gaseous H$_2$) is attributed to a weakly adsorbed hydride. Bands II and III at 2045 and 1990 cm^{-1} (the latter appearing as a shoulder of the former) are assigned to strongly adsorbed hydrides differing in terms of their local environment. Finally, the weaker bands IVa and IVb at about 1865 and 1740 cm^{-1} are assigned to interfacial Pt–H species, *i.e.* linear hydrides formed at Pt atoms in direct interaction with the alumina support. The assignments are
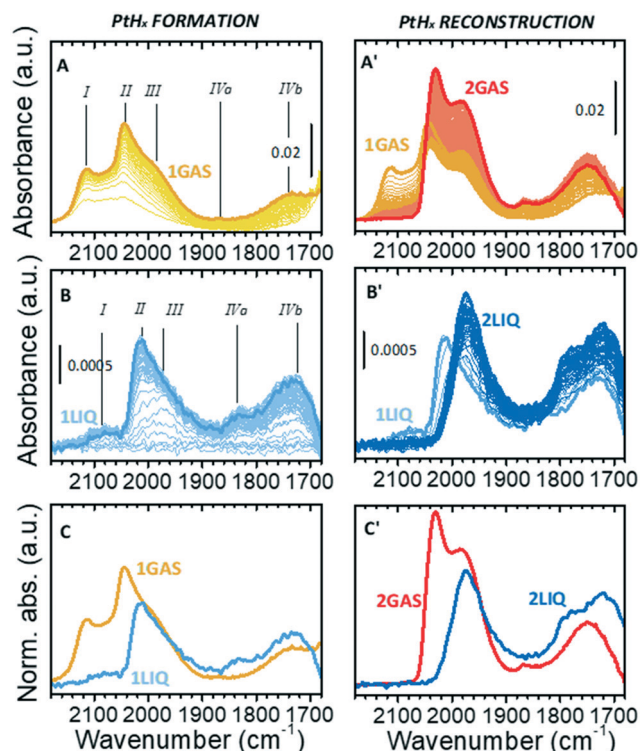
Fig. 2 (A) Evolution of the IR spectra in the region characteristic of the v(Pt–H) vibrational modes for linear Pt–H species during the gas-phase reduction of Pt/Al$_2$O$_3$ in N$_2$/H$_2$ at 70 °C. Spectrum 1GAS was collected after 10 min in N$_2$/H$_2$ flow. (A') Evolution of the IR spectra during the successive H$_2$ desorption in N$_2$ flow at 70 °C, up to the maximum intensities of the v(Pt–H) bands. Spectrum 2GAS was collected after about 1 h in desorption conditions. (B) and (B') are the same as (A) and (A') for the ATR-IR experiment performed in liquid phase. Spectrum 1LIQ was collected after about 1 h in hydrogenation conditions, while spectrum 2LIQ after about 1 h in inert conditions. (C) Comparison of the final spectra reported in (A) and (B). (C') Comparison of the final spectra reported in (A') and (B').

summarized in Table 1. All the five bands gradually intensified over time almost at the same rate and reached a steady condition after about 10 min (spectrum 1GAS). At that point H$_2$ was removed from the flow, and the desorption process was monitored (Fig. 2A'). Band I rapidly disappeared,

while the other bands evolved in a counterintuitive way. The intensity of bands II and III passed through a minimum and then rose, while that of bands IVa and IVb increased constantly. These v(Pt–H) bands reached their maximum intensity after about 1 h (spectrum 2GAS) and then they all vanished rapidly, following the observations reported in our previous work.[49]

This counterintuitive behavior is the same observed for the same sample measured in the presence of H$_2$ at 120 °C, that was explained with a reconstruction of the hydrogenated Pt nanoparticles driven by a change in the H-coverage.[49] Several theoretical models predict the occurrence of this phenomenon for Pt particles of subnanometric and nanometric size, which is also in accordance with experimental structural data obtained by XAS.[15,16,21,24,25,27,34] According to theoretical models, at high H-coverage Pt$_{13}$ nanoparticles adopt preferentially a cuboctahedral geometry poorly interacting with the support because they are H-solvated, mainly by multi-folded hydrides which are not visible by IR spectroscopy. Upon decreasing the H-coverage, the Pt$_{13}$ nanoparticles reconstruct into a biplanar geometry strongly interacting with the support, which is accompanied by a conversion of multi-folded hydrides into linear ones, thus explaining the intensification of the v(Pt–H) bands in the IR spectrum.

Fig. 2B and B' show the results of the same experiment performed in liquid phase. The evident similarity to the gas-phase experiment allows us to translate the assignment of the observed signals to Pt–H species (Table 1). Focusing the attention on the hydrides formation step (Fig. 2B), from a qualitative perspective the ATR-IR spectra possess the same profile of those collected in the gas-phase (Fig. 2A), but there are important differences in the position, relative intensity and temporal evolution of the bands. Band I was barely present in cyclohexane (2088 cm^{-1}); band II was less intense and red-shifted by *ca.* 25 cm^{-1}; band IVa was more evident and red-shifted by *ca.* 30 cm^{-1}, while bands III and IVb remained unaffected. Moreover, the five bands did not grow simultaneously as observed in the gas-phase experiment: band III was the first one to appear, followed by band II. In general, the kinetics of hydrides formation in the liquid-

Table 1 Assignment of the vibrational modes of Pt–hydride and Pt–carbonyl species on Pt/Al$_2$O$_3$ in the gas-phase experiment as well as in cyclohexane. The reported frequencies (in cm^{-1}) of PtH$_x$ refer to 1GAS and 1LIQ spectra of Fig. 2A and B. The reported frequencies of Pt–carbonyls refer to the maximum CO-coverage obtained under the conditions adopted in this work (Fig. 4)

Linear Pt–hydrides, v(Pt–H)					
	Species I	Species II	Species III	Species IVa and IVb	
Gas-phase	2115	2045	1990	1865 and 1740	
Cyclohexane	2088	2020	1990	1835 and 1740	

Pt–Carbonyls, v(Pt–CO)					
	Linear Pt–carbonyls			Multi-folded Pt–carbonyls		
	Terrace sites (L1)	Edge sites (L2)	Corner sites (L3)	Bridged on terraces (B1)	Bridged on edges (B2)	3-Fold (B3)
Gas-phase	2088	2070	2010	1878	1830	1790
Cyclohexane	2080	2060	—	1862	1818	—

phase was slower than in the gas-phase, likely as a consequence of the low H_2 concentration in cyclohexane, which is dictated by its solubility, and its higher diffusion limitation from the liquid-phase onto the catalyst surface than in the gas-phase. A direct comparison of the two final spectra collected in the presence of H_2 is provided in Fig. 2C.

The differences between gas-phase and liquid-phase experiments are even larger when looking at the evolution of the IR spectra during the desorption step in cyclohexane (Fig. 2B'). Band I rapidly disappeared, while band II was quickly converted into band III within a few minutes as indicated by the formation of an isosbestic point at 1988 cm^{-1}. At longer time, only a constant drift in the baseline was observed without further evolution in the position and/or intensity of the bands. The kinetics involved is very different from that observed in the gas-phase: the conversion of species II into species III is very fast and the spectra do not change further even after a very prolonged treatment in Ar-saturated solvent, while in the gas-phase the increase in intensity of species II and III is much slower. The final spectrum (2LIQ) is compared in Fig. 2C' to that corresponding to the maximum intensity of the $v(Pt–H)$ bands obtained under gas-phase conditions (spectrum 2GAS). The complete absence of band II in the ATR-IR spectrum is the major difference between the two experiments. It is important to notice that, within the time interval investigated, the Pt–H bands did not disappear, in contrast to what was observed in the gas-phase and already reported in our previous work.[49] This indicates that cyclohexane stabilizes the Pt nanoparticles in a hydrogenated form even in absence of hydrogen, preventing their reconstruction.

The set of data reported in Fig. 2 reveals that the presence of the solvent alters the relative distribution of the Pt–H species with respect to the gas-phase situation, both during the Pt oxide reduction and during the H_2 desorption steps. We find at least two possible explanations for this behavior, which are not mutually exclusive: i) in the presence of the solvent, the overall H-coverage is lower than in gas-phase, either because the solvent competes with hydrogen in the occupancy of the adsorption sites and/or because the morphology of the Pt nanoparticles is different in the two cases; ii) under these conditions, in liquid-phase Pt is not completely reduced, which also leads to an overall lower H-coverage. In support of hypothesis i) it must be noticed that the evolution of the ATR-IR spectra in liquid-phase during the desorption step is very much similar to what occurs during the catalytic hydrogenation of toluene in vapour-phase,[49] and is ascribed to a competitive adsorption between hydrogen and toluene. In support of hypothesis ii) there is the experimental evidence that the Pt phase is indeed not fully reduced in liquid-phase at 70 °C (as demonstrated in the following section).

Another relevant effect of the solvent is the stabilization of the Pt nanoparticles in a H-solvated form even in the absence of H_2. This appears particularly relevant during reaction. In

the case the reaction environment becomes poor in H_2, the solvent can disfavour hydrogen desorption and decrease the rate of the morphologic reconstruction the Pt nanoparticles experience in the gas phase.[16,21,22,24,25,27] We speculate that in this situation, the catalyst could sustain a reaction for longer time.

3.2 CO adsorption at room temperature

The surface properties of the Pt nanoparticles were successively investigated by means of CO adsorption at room temperature, which is one of the most utilized methods for the characterization of metal surfaces and of metal nano-particles.[68–84] Fig. 3 shows the sequence of transmission IR spectra collected upon progressive CO adsorption on Pt/Al_2O_3 in the gas-phase (Fig. 3A and B) and in the liquid-phase (Fig. 3C and D) in two different spectral regions, namely the $v(CO)$ region (Fig. 3A and C) and the region characteristic of surface carbonates (Fig. 3B and D).

The sequence of IR spectra collected upon increasing the CO coverage (θ_{CO}) in gas-phase is complex. More in detail, a total of six bands was observed in the $v(CO)$ region (Fig. 3A), which shift in position and grow at a different rate upon increasing the CO partial pressure. Bands in the 2100–1900 cm^{-1} region (L1, L2 and L3) are characteristic of linear Pt–carbonyls, while those in 1900–1700 cm^{-1} (B1, B2 and B3) are characteristic of multi-coordinated Pt–carbonyls. These bands can be assigned on the basis of surface science studies,[68–73] as well as of the abundant literature on CO adsorption over Pt-based heterogeneous catalysts[75,77–80] as follows (Table 1).

– Band L1 at 2077 cm^{-1} at low θ_{CO} and at 2088 cm^{-1} at high θ_{CO}, is attributed to CO linearly adsorbed at terrace sites.[73–76,85]

– Band L2 at 2060 cm^{-1} at low θ_{CO} and at 2070 cm^{-1} at high θ_{CO}, is due to CO adsorbed at the particles edges.[73,85–89]

– The very broad band L3 centered at $ca.$ 2010 cm^{-1}, which does not shift with θ_{CO}, is ascribed to CO adsorbed at particles corners/kinks.[85,87]

– Band B1 at 1878 cm^{-1} and band B2 at $ca.$ 1830 cm^{-1}, which are almost insensitive to θ_{CO}, are assigned to bridged carbonyls on terraces and edges, respectively.[86,88–90]

– The broad band B3 at $ca.$ 1790 cm^{-1} is attributed to 3-fold coordinated CO at hollow sites.[62,80,86,90,91]

A rapid inspection of the spectra as a whole suggests a predominance of defects (edges and corners/kinks) rather than extended terraces, as expected because of the very high metal dispersion.

When analyzing the whole sequence of spectra as a function of θ_{CO} in a narrower spectral range, additional relevant information can be obtained. After the very first small pulses of CO, L1 and L2 were the first bands to appear, immediately followed by L3; bands due to bridged species appeared later. Upon increasing θ_{CO}, all the bands intensified, but did not shift until $P_{He/CO}$ of about 2 mbar (bold orange spectrum in Fig. 3A). At this point, band L1 stopped growing and blue-shifted, band L2 blue-shifted while
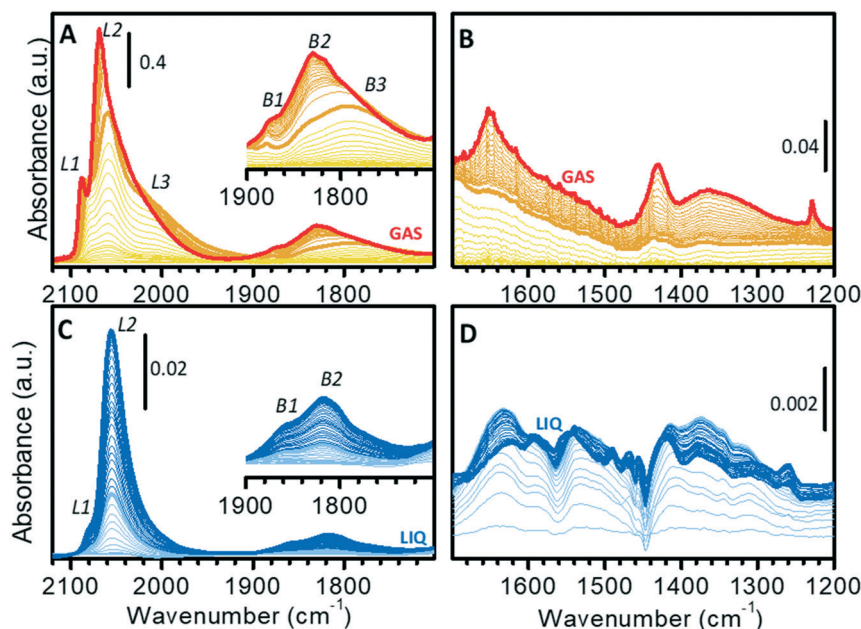
This journal is © The Royal Society of Chemistry 2022

Catal. Sci. Technol., 2022, **12**, 1359–1367 | **1363**

Fig. 3 (A) FT-IR spectra of CO adsorbed at room temperature on Pt/Al_2O_3 (activated and reduced at 70 °C in gas-phase) in the $v(CO)$ region and (B) in the 1700–1200 cm^{-1} region, where the bands typical for surface carbonates are observed. The bold orange spectrum in (A) and (B) ($P_{He/CO}$ = 2 mbar) is the last one before observing the upward shift of bands L1 and L2 (see text). (C) ATR-IR spectra of CO adsorbed at room temperature on Pt/Al_2O_3 (activated and reduced at 70 °C in liquid-phase) in the presence of cyclohexane in the $v(CO)$ region and (D) in the 1700–1200 cm^{-1} region. The bold light blue spectrum in (C) and (D) is that where the bands in 1700–1200 cm^{-1} region are maximized. The insets in (A) and (C) show a magnification of the 1900–1700 cm^{-1} region.

still growing and band L3 slightly attenuated. In the region of multi-folded carbonyls, bands B1 and B3 did not grow further, while band B2 became dominant. The blue-shift of bands L1 and L2 is explained in terms of a strong dipole–dipole coupling interaction between adjacent CO molecules at high θ_{CO}. The attenuation of band L3 and the simultaneous intensification of band L2 is well explained by the "transfer of intensity" concept proposed by Hollins:[92] in the presence of strong dipole–dipole coupling involving more than one adsorbed species, a transfer of intensity may take place from a band at lower frequency to a band at higher frequency.

It is worth mentioning that, at the same time, in the 1700–1200 cm^{-1} region (Fig. 3B) a few bands started growing at *ca.* 1650, 1440 and 1230 cm^{-1}. These bands are readily assigned to the $v(CO)$ and $\delta(OH)$ vibrational modes of a family of bicarbonates typically formed on alumina activated at low temperature.[93] Interestingly, bicarbonates formed only when θ_{CO} was high enough to determine a coupling interaction among adsorbed CO (from bold orange spectra in Fig. 3B). We hypothesize that they are the result of disproportionation of two neighboring adsorbed CO molecules, which give CO_2 (stabilized as bicarbonate at the partially hydrated surface of alumina) and adsorbed carbon. As a final observation, the fact that carbonate formation was not observed at low θ_{CO} confirms that the Pt phase was completely reduced, despite the low reduction temperature (70 °C). With reference to the TPR curve of Fig. 1C, this means that full reduction of the Pt–oxide phase can be

achieved in the gas-phase even below 130 °C, provided that the reduction time is sufficiently long.

Fig. 3C and D show the results of a similar experiment performed in the liquid-phase, where the spectra were collected as a function of exposure time of the catalyst to a flow of CO-saturated cyclohexane. In this case, the gradual increase in θ_{CO} is also affected by the diffusion of CO from the solvent to the catalyst. In the $v(CO)$ region (Fig. 3C), the evolution of the spectra was much simpler than in the gas-phase. Contrary to what observed in gas-phase, the $v(CO)$ bands intensified at the same rate and did not shift until reaching saturation (Fig. 3C). This indicates that when the catalyst is in the liquid environment under these experimental conditions, dipole–dipole coupling between adsorbed CO molecules is not favored and thus the overall θ_{CO} is much lower than in the absence of the solvent. Nevertheless, these spectra are not the same as those collected in gas-phase at very low θ_{CO}, the most striking difference being the almost total absence of bands L3 and B3. In the carbonates region (broad signals in the 1700–1200 cm^{-1} region; Fig. 3D) the spectra are more complex than in gas-phase and the appearance of carbonate species already in the early stages of CO adsorption reveals the occurrence of a rich chemistry. Observation of carbonates as soon as CO reached the sample is a strong indication that the Pt phase was not fully reduced after the reduction at 70 °C in the liquid-phase. CO reduced this fraction of oxidized Pt with the consequent production of CO_2, which is stabilized by the alumina support as carbonate (light blue spectra in Fig. 3D).

This demonstrates that H_2-reduction at 70 °C was less efficient in the presence of cyclohexane than in the gas-phase. The poor solubility of H_2 in cyclohexane is a possible explanation, but we cannot exclude that the geometry of the ATR-IR cell, in which the solvent mostly by-passes the catalyst layer, could also play an important role. Formation of carbonates was completed after a few minutes, while Pt–carbonyls kept growing for longer time. Finally, it is worth noticing that in the liquid-phase experiment the simultaneous growth of carbonates and carbonyls as well as the shiftless growth of signals of carbonyls indicate that disproportionation of CO and the consequent formation of carbonates did not occur, thus confirming that disproportionation requires two vicinal adsorbed CO molecules as it was observed in the spectra collected in gas-phase.

Fig. 4 compares the IR spectra collected at the maximum θ_{CO} in the two experiments in the gas-phase and in the liquid-phase. It is evident that the spectrum of CO adsorbed on Pt/Al_2O_3 in cyclohexane is simpler than that of CO adsorbed in the gas-phase, with only two bands in the region of linear carbonyls, and two bands in the region of bridged carbonyls. Bands L1 and L2 are observed at 2080 and 2060 cm^{-1} in the liquid phase experiment, which are the values expected for linearly adsorbed CO on terraces and edges when isolated; moreover, the relative intensity of band L1 is much lower than in spectrum GAS and bands L3 and B3 are absent. All these observations suggest that the adsorption sites located at the flat domains of the nanoparticles (bands L1 and B3), as well as on corners/kinks (band L3), are less accessible to CO in the presence of the solvent, which forces CO to adsorb prevalently at the edges (bands L2 and B2). This suggests that in the presence of the solvent there are less sites available for CO adsorption, most likely because the solvent competes with CO for adsorption on the Pt surface.[68]

Finally, we should note that we have performed a purely qualitative study. We do not have yet the elements to compare quantitatively the coverages of CO and hydrides in the two different environments. We have to consider that a direct comparison of the intensities associated with adsorbed CO species in the gas and in the liquid phases cannot be performed, because of the different environment, optical geometries of the experiments and CO-coverage (likely lower in liquid-phase because of the competitive effect of the solvent). In order to proceed to a reliable quantitative prediction, the degree of the CO-coverage under the adopted experimental conditions, the metal surface area and the relative proportion of the different families of binding sites, as well as their energetics and the extinction coefficients of all the adsorbed species, should be known exactly. The data presented here allows us to qualitatively describe the surface sites available at the Pt nanoparticles and to predict which sites are favored in the liquid environment by comparing the differences in the relative intensities in the two cases.

4. Conclusions

In this work, we aimed at bridging the gap of knowledge of the adsorption phenomena occurring at the solid–gas and the solid–liquid interfaces. To this end, we investigated the adsorption of H_2 and CO over an industrial Pt/Al_2O_3 catalyst using transmission IR spectroscopy in gas-phase and ATR-IR spectroscopy in the liquid-phase.

We found that reduction by H_2 at 70 °C is less efficient in the presence of the solvent (in this case, cyclohexane) than in the gas-phase, probably due to the poor H_2 solubility in cyclohexane and/or to the particular geometry of the spectroscopy cell used to analyze the solid–liquid interface. Contrary to gas-phase case, the solvent stabilizes the Pt nanoparticles in a partially hydrogenated form even in the absence of H_2, preventing their complete reconstruction. Not only the Pt–H species stability is affected, but also their relative distribution. This suggests that the solvent competes with H_2 for the occupation of the surface sites, thus determining an overall lower H_2 coverage. Competition between the solvent and the adsorbing molecule was also observed in the case of CO. A careful comparison of the transmission and ATR-IR spectra of adsorbed CO allowed us to conclude that the adsorption sites located at the terraces as well as on kinks are less accessible to CO in the presence of the solvent. Therefore, CO adsorbs prevalently at the edges of the Pt nanoparticles. This different behavior may bear important implications for the reactivity of the Pt nanoparticles in heterogeneously catalyzed reactions in the gas- and in the liquid-phase.

Conflicts of interest

There are no conflicts to declare.
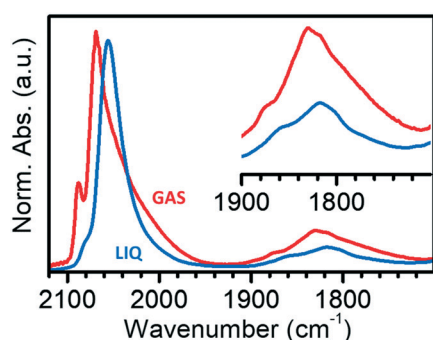
Acknowledgements

Fig. 4 IR spectra of CO adsorbed at room temperature on Pt/Al_2O_3 activated and reduced at 70 °C in gas-phase (GAS) and in liquid-phase (LIQ) in the ν(CO) region. The inset reports a magnification of the 1900–1700 cm^{-1} region of multi-coordinated carbonyls. Spectra GAS and LIQ were arbitrarily normalized to the intensity of band L2.

References

1 R. L. Augustine, *Heterogeneous Catalysis for the Synthetic Chemist*, Dekker, New York, 1995.

2 G. M. Loudon, *Organic Chemistry*, Benjamin/Cummings Pub. Co., Menlo Park, 2nd edn, 1988.

3 S. Nishimura, *Handbook of Heterogeneous Catalytic Hydrogenation for Organic Synthesis*, Wiley, Chichester, 2001.

4 P. N. Rylander, *Best Synthetic Methods: Hydrogenation Methods*, Academic Press, London, 1985.

5 M. Che, *Catal. Today*, 2013, **218–219**, 162–171.

6 A. Zecchina and S. Califano, Chapter 1 – From the Onset to the First Large-Scale Industrial Processes, in *The Development of Catalysis: A History of Key Processes and Personas in Catalytic Science and Technology*, ed. I. John, Wiley & Sons, 2017, ch. 1, pp. 1–57, DOI: 10.1002/9781119181286.

7 A. I. Frenkel, M. W. Small, J. G. Smith, R. G. Nuzzo, K. O. Kvashnina and M. Tromp, *J. Phys. Chem. C*, 2013, **117**, 23286–23294.

8 A. I. Frenkel, C. W. Hills and R. G. Nuzzo, *J. Phys. Chem. B*, 2001, **105**, 12689–12703.

9 J.-D. Grunwaldt and B. S. Clausen, *Top. Catal.*, 2002, **18**, 37–43.

10 M. A. Newton, B. Jyoti, A. J. Dent, S. G. Fiddy and J. Evans, *Chem. Commun.*, 2004, 2382–2383, DOI: 10.1039/b405694a.

11 G. Agostini, R. Pellegrini, G. Leofanti, L. Bertinetti, S. Bertarione, E. Groppo, A. Zecchina and C. Lamberti, *J. Phys. Chem. C*, 2009, **113**, 10485–10492.

12 R. Arrigo, K. Badmus, F. Baletto, M. Boeije, M. Bowker, K. Brinkert, A. Bugaev, V. Bukhtiyarov, M. Carosso, R. Catlow, R. Chanerika, P. R. Davies, W. Dononelli, H. J. Freund, C. Friend, S. Gallarati, B. Gates, A. Genest, E. K. Gibson, J. Hargreaves, S. Helveg, H. Huang, G. Hutchings, N. Irvine, R. Johnston, S. Lai, C. Lamberti, J. Macginley, D. Marchant, T. Murayama, R. Nome, Y. Odarchenko, J. Quinson, S. Rogers, A. Russell, S. Said, P. Sermon, P. Shah, S. Simoncelli, K. Soulantica, F. Spolaore, B. Tooze, L. Torrente-Murciano, A. Trunschke, D. Willock and J. Zhang, *Faraday Discuss.*, 2018, **208**, 339–394.

13 J. H. Kang, L. D. Menard, R. G. Nuzzo and A. I. Frenkel, *J. Am. Chem. Soc.*, 2006, **128**, 12068–12069.

14 M. W. Small, S. I. Sanchez, N. S. Marinkovic, A. I. Frenkel and R. G. Nuzzo, *ACS Nano*, 2012, **6**, 5583–5595.

15 L.-L. Wang and D. D. Johnson, *J. Am. Chem. Soc.*, 2007, **129**, 3658–3664.

16 C. Mager-Maury, G. Bonnard, C. Chizallet, P. Sautet and P. Raybaud, *ChemCatChem*, 2011, **3**, 200–207.

17 O. S. Alexeev, F. Li, M. D. Amiridis and B. C. Gates, *J. Phys. Chem. B*, 2005, **109**, 2338–2349.

18 E. Bus and J. A. van Bokhoven, *Phys. Chem. Chem. Phys.*, 2007, **9**, 2894–2902.

19 L. Li, L.-L. Wang, D. D. Johnson, Z. Zhang, S. I. Sanchez, J. H. Kang, R. G. Nuzzo, Q. Wang, A. I. Frenkel, J. Li, J. Ciston, E. A. Stach and J. C. Yang, *J. Am. Chem. Soc.*, 2013, **135**, 13062–13072.

20 S. I. Sanchez, L. D. Menard, A. Bram, J. H. Kang, M. W. Small, R. G. Nuzzo and A. I. Frenkel, *J. Am. Chem. Soc.*, 2009, **131**, 7040–7054.

21 W. Zhao, C. Chizallet, P. Sautet and P. Raybaud, *J. Catal.*, 2019, **370**, 118–129.

22 C. Dessal, A. Sangnier, C. Chizallet, C. Dujardin, F. Morfin, J. L. Rousset, M. Aouine, M. Bugnet, P. Afanasiev and L. Piccolo, *Nanoscale*, 2019, **11**, 6897–6904.

23 L. Piccolo, *Catal. Today*, 2021, **373**, 80–97.

24 C. Chizallet and P. Raybaud, *Catal. Sci. Technol.*, 2014, **4**, 2797–2813.

25 A. Gorczyca, V. Moizan, C. Chizallet, O. Proux, W. Del Net, E. Lahera, J.-L. Hazemann, P. Raybaud and Y. Joly, *Angew. Chem., Int. Ed.*, 2014, **53**, 12426–12429.

26 G. Sun, A. N. Alexandrova and P. Sautet, *J. Chem. Phys.*, 2019, **151**, 1–15.

27 P. Raybaud, C. Chizallet, H. Toulhoat and P. Sautet, *Phys. Chem. Chem. Phys.*, 2012, **14**, 16773–16774.

28 G. S. Erfani, S. Hong and T. S. Rahman, *J. Phys. Chem. C*, 2019, **123**, 16893–16901.

29 F. W. Lytle, P. S. P. Wei, R. B. Greegor, G. H. Via and J. H. Sinfelt, *J. Chem. Phys.*, 1979, **70**, 4849–4855.

30 M. Vaarkamp, J. T. Miller, F. S. Modica and D. C. Koningsberger, *J. Catal.*, 1996, **163**, 294–305.

31 D. E. Ramaker, B. L. Mojet, M. T. Garriga Oostenbrink, J. T. Miller and D. C. Koningsberger, *Phys. Chem. Chem. Phys.*, 1999, **1**, 2293–2302.

32 A. L. Ankudinov, J. J. Rehr, J. J. Low and S. R. Bare, *Phys. Rev. Lett.*, 2002, **89**, 139702-1.

33 D. C. Koningsberger, M. K. Oudenhuijzen, J. De Graaf, J. A. Van Bokhoven and D. E. Ramaker, *J. Catal.*, 2003, **216**, 178–191.

34 M. K. Oudenhuijzen, J. A. van Bokhoven, J. T. Miller, D. E. Ramaker and D. C. Koningsberger, *J. Am. Chem. Soc.*, 2005, **127**, 1530–1540.

35 E. Bus, J. T. Miller, A. J. Kropf, R. Prins and J. A. van Bokhoven, *Phys. Chem. Chem. Phys.*, 2006, **8**, 3248–3258.

36 E. Bus, J. T. Miller and J. A. van Bokhoven, *J. Phys. Chem. B*, 2005, **109**, 14581–14587.

37 J. P. Candy, P. Fouilloux and M. Primet, *Surf. Sci.*, 1978, **72**, 167–176.

38 L. T. Dixon, R. Barth and J. W. Gryder, *J. Catal.*, 1975, **37**, 368–375.

39 D. D. Eley, D. M. Moran and C. H. Rochester, *Trans. Faraday Soc.*, 1968, **64**, 2168–2180.

40 W. A. Pliskin and R. P. Eischens, *Z. Phys. Chem.*, 1960, **24**, 11–23.

41 M. Primet, J. M. Basset, M. V. Mathieu and M. Prettre, *J. Catal.*, 1973, **28**, 368–375.

42 T. Szilagyi, *J. Catal.*, 1990, **121**, 223–227.

43 D. Paleček, G. Tek, J. Lan, M. Iannuzzi and P. Hamm, *J. Phys. Chem. Lett.*, 2018, **9**, 1254–1259.

44 P. Albers, E. Auer, K. Ruth and S. F. Parker, *J. Catal.*, 2000, **196**, 174–179.

45 P. W. Albers, M. Lopez, G. Sextl, G. Jeske and S. F. Parker, *J. Catal.*, 2004, **223**, 44–53.

1366 | *Catal. Sci. Technol.*, 2022, **12**, 1359–1367

This journal is © The Royal Society of Chemistry 2022

46 H. Asada, T. Toya, H. Motohashi, M. Sakamoto and Y. Hamaguchi, *J. Chem. Phys.*, 1975, **63**, 4078–4079.

47 S. F. Parker, C. D. Frost, M. Telling, P. Albers, M. Lopez and K. Seitz, *Catal. Today*, 2006, **114**, 418–421.

48 A. J. Renouprez and H. Jobic, *J. Catal.*, 1988, **113**, 509–516.

49 M. Carosso, E. Vottero, A. Lazzarini, S. Morandi, M. Manzoli, K. A. Lomachenko, M. J. Ruiz, R. Pellegrini, C. Lamberti, A. Piovano and E. Groppo, *ACS Catal.*, 2019, **9**, 7124–7136.

50 J.-P. Candy, P. Fouilloux and M. Primet, *Surf. Sci.*, 1978, **72**, 167–176.

51 D. Ferri, Toward operando infrared spectroscopy of heterogeneous catalysts, in *Heterogeneous catalysts: Emerging techniques for design, characterization and applications*, ed. A. U. W. Y. Teoh, Y. H. Ng and P. Sit, Wiley-VCH GmbH, 2021, pp. 311–338, DOI: 10.1002/9783527813599.ch18.

52 T. Bürgi and A. Baiker, *Adv. Catal.*, 2006, **50**, 227–283.

53 T. Bürgi, R. Wirz and A. Baiker, *J. Phys. Chem. B*, 2003, **107**, 6774–6781.

54 G. M. Hamminga, G. Mul and J. A. Moulijn, *Chem. Eng. Sci.*, 2004, **59**, 5479–5485.

55 A. Pintar, R. Malacea, C. Pinel, G. Fogassy and M. Besson, *Appl. Catal., A*, 2004, **264**, 1–12.

56 J. E. Rekoske and M. A. Barteau, *Ind. Eng. Chem. Res.*, 1995, **34**, 2931–2939.

57 Z. Wang, M. L. Larsson, M. Grahn, A. Holmgren and J. Hedlund, *Chem. Commun.*, 2004, 2888–2889, DOI: 10.1039/b410314a.

58 D. Ferri and A. Baiker, *Top. Catal.*, 2009, **52**, 1323–1333.

59 C. Boulho, E. K. Gibson, M. I. McAllister, R. Moss and D. Lennon, *Top. Catal.*, 2020, **63**, 386–393.

60 R. He, R. R. Davda and J. A. Dumesic, *J. Phys. Chem. B*, 2005, **109**, 2810–2820.

61 S. D. Ebbesen, B. L. Mojet and L. Lefferts, *J. Catal.*, 2007, **246**, 66–73.

62 D. Ferri, T. Bürgi and A. Baiker, *J. Phys. Chem. B*, 2001, **105**, 3187–3195.

63 I. Ortiz-Hernandez, D. J. Owens, M. R. Strunk and C. T. Williams, *Langmuir*, 2006, **22**, 2629–2639.

64 K. M. Kaprielova, O. A. Yakovina, I. I. Ovchinnikov, S. V. Koscheev and A. S. Lisitsyn, *Appl. Catal., A*, 2012, **449**, 203–214.

65 J. E. Benson and M. Boudart, *J. Catal.*, 1965, **4**, 704–710.

66 M. Carosso, E. Vottero, S. Morandi, M. Manzoli, D. Ferri, T. Fovanna, R. Pellegrini, A. Piovano and E. Groppo, *ChemCatChem*, 2021, **13**, 900–908.

67 J. B. Brazier, B. N. Nguyen, L. A. Adrio, E. M. Barreiro, W. P. Leong, M. A. Newton, S. J. A. Figueroa, K. Hellgardt and K. K. M. Hii, *Catal. Today*, 2014, **229**, 95–103.

68 A. Crossley and D. A. King, *Surf. Sci.*, 1977, **68**, 528–538.

69 B. E. Heyden and A. M. Bradshaw, *Surf. Sci.*, 1983, **125**, 787–802.

70 B. E. Hayden, K. Kretzschmar, A. M. Bradshaw and R. G. Greenler, *Surf. Sci.*, 1985, **149**, 394–406.

71 A. M. Bradshaw and F. M. Hoffmann, *Surf. Sci.*, 1978, **72**, 513–535.

72 G. Ertl, M. Neumann and K. M. Streit, *Surf. Sci.*, 1977, **64**, 393–410.

73 R. K. Brandt, M. R. Hughes, L. P. Bourget, K. Truszkowska and R. G. Greenler, *Surf. Sci.*, 1993, **286**, 15–25.

74 P. Pillonel, S. Derrouiche, A. Bourane, F. Gaillard, P. Vernoux and D. Bianchi, *Appl. Catal., A*, 2005, **278**, 223–231.

75 S. K. Cheah, V. P. Bernardet, A. A. Franco, O. Lemaire and P. Gelin, *J. Phys. Chem. C*, 2013, **117**, 22756–22767.

76 T. Avanesian, S. Dai, M. J. Kale, G. W. Graham, X. Pan and P. Christopher, *J. Am. Chem. Soc.*, 2017, **139**, 4551–4558.

77 J. A. Anderson, F. K. Chong and C. H. Rochester, *J. Mol. Catal. A: Chem.*, 1999, **140**, 65–80.

78 R. Barth, R. Pitchai, R. L. Anderson and X. E. Verykios, *J. Catal.*, 1989, **116**, 61–70.

79 P. Bazin, O. Saur, J. C. Lavalley, M. Daturi and G. Blanchard, *Phys. Chem. Chem. Phys.*, 2005, **7**, 187–194.

80 D. M. Haaland, *Surf. Sci.*, 1987, **185**, 1–14.

81 F. Zaera, *ChemCatChem*, 2012, **4**, 1525–1533.

82 T. Elgayyar, R. Atwi, A. Tuel and F. C. Meunier, *Catal. Today*, 2021, **373**, 59–68.

83 C. Lentz, S. P. Jand, J. Melke, C. Roth and P. Kaghazchi, *J. Mol. Catal. A: Chem.*, 2017, **426**, 1–9.

84 I. Jbir, A. Paredes-Nunez, S. Khaddar-Zine, Z. Ksibir, F. Meunier and D. Bianchi, *Appl. Catal., A*, 2015, **505**, 309–318.

85 F. Coloma, J. M. Coronado, C. H. Rochester and J. A. Anderson, *Catal. Lett.*, 1998, **51**, 155–162.

86 A. Bourane, O. Dulaurent and D. Bianchi, *J. Catal.*, 2000, **196**, 115–125.

87 J. Rasko, *J. Catal.*, 2003, **217**, 478–486.

88 J. Xu and J. T. Yates Jr., *J. Chem. Phys.*, 1993, **99**, 725–732.

89 J. Xu and J. T. Yates Jr., *Surf. Sci.*, 1995, **327**, 193–201.

90 B. E. Hayden and A. M. Bradshaw, The Adsorption of CO on Pt(111) Studied by Infrared-Reflection-Adsorption Spectroscopy, in *Stud. Surf. Sci. Catal.*, ed. C. R. Brundle and H. Morawitz, Elsevier, 1983, vol. 14, p. 51.

91 N. P. Lebedeva, A. Rodes, J. M. Feliu, M. T. M. Koper and R. A. van Santen, *J. Phys. Chem. B*, 2002, **106**, 9863–9872.

92 P. Hollins, *Surf. Sci. Rep.*, 1992, **16**, 51–94.

93 C. Morterra and G. Magnacca, *Catal. Today*, 1996, **27**, 497–532.

94 S. D. Ebbesen, B. L. Mojet and L. Lefferts, *Langmuir*, 2006, **22**, 1079–1085.

This journal is © The Royal Society of Chemistry 2022

Catal. Sci. Technol., 2022, **12**, 1359–1367 | 1367